# Do globular clusters possess Dark Matter halos? A case study in NGC 2419

R. Ibata $^{1\star}$ , C. Nipoti $^{2}$ , A. Sollima $^{3}$ , M. Bellazzini $^{4}$ , S.C. Chapman $^{5}$  and E. Dalessandro $^{2}$ 

- <sup>1</sup>Observatoire Astronomique, Université de Strasbourg, CNRS, 11, rue de l'Université, F-67000 Strasbourg, France
- <sup>2</sup>Department of Physics and Astronomy, viale Berti Pichat, 6/2, I-40127 Bologna, Italy
- <sup>3</sup> INAF Osservatorio Astronomico di Padova, vicolo dell'Osservatorio 5, 35122, Padova, Italy
- $^4$  INAF-Bologna Astronomical Observatory, via Ranzani 1, I-40127 Bologna, Italy
- <sup>5</sup> Institute of Astronomy, Madingley Road, Cambridge CB3 0HA, UK

September 18, 2012

# ABSTRACT

We use recently published measurements of the kinematics, surface brightness and stellar mass-to-light ratio of the globular cluster NGC 2419 to examine the possibility that this Galactic halo satellite is embedded in a low-mass dark matter halo. NGC 2419 is a promising target for such a study, since its extreme Galactocentric distance and large mass would have greatly facilitated the retention of dark matter. A Markov-Chain Monte Carlo approach is used to investigate composite dynamical models containing a stellar and a dark matter component. We find that it is unlikely that a significant amount of dark matter ( $\lesssim 6\%$  of the luminous mass inside the tidal limit of the cluster) can be present if the stars follow an anisotropic Michie model and the dark matter a double power law model. However, we find that more general models, derived using a new technique we have developed to compute non-parametric solutions to the spherical Jeans equation, suggest the presence of a significant dark matter fraction (approximately twice the stellar mass). Thus the presence of a dark matter halo around NGC 2419 cannot be fully ruled out at present, yet any dark matter within the 10' visible extent of the cluster must be highly concentrated and cannot exceed 1.1  $\times$  $10^6 M_{\odot}$  (99% confidence), in stark contrast to expectations for a plausible progenitor halo of this structure.

**Key words:** globular clusters: individual (NGC 2419) — dark matter — stellar dynamics

#### 1 INTRODUCTION

Dwarf spheroidal galaxies (dSphs) and globular clusters (GCs) have similar luminosities but are strikingly different in terms of their dark-matter (DM) content, as inferred from the kinematics of their stars: while dSphs (and their "ultrafaint" extension to low luminosity) galaxies are the most DM dominated systems, there is virtually no evidence that GCs have DM halos (Heggie & Hut 1996; Mashchenko & Sills 2005a; Bradford et al. 2011). This finding might represent a problem for standard cold dark matter cosmology, in which GCs are expected to form within their own DM halos (Peebles 1984). However it is quite possible that GCs were originally embedded in massive DM halos that evolved during the cluster lifetime as a consequence of interaction with the cluster stars (Baumgardt & Mieske 2008) and stripping

by the tidal field of the host galaxy (Mashchenko & Sills 2005b; Saitoh et al. 2006). Therefore, the central parts of GCs might be left relatively poor in DM, because the DM at the present time either populates the outer region of the cluster or has been stripped (Bekki & Yong 2012). However, this is unlikely to be the case in GCs observed to have stellar tidal tails, which argue against very extended massive DM components (Moore 1996). While it is not well established to what extent two-body relaxation and tidal stripping are effective in shaping hypothetical DM halos of GCs, it is clear that these effects are minimized in clusters with long twobody relaxation time and that orbit the outer parts of the host galaxy, where tidal effects are small. The prototype of these systems is the remote massive GC NGC 2419, located in the halo of the Milky Way at a distance of d = 87.5 kpc (Di Criscienzo et al. 2011) (Galactocentric distance of  $\sim 95 \,\mathrm{kpc}$ ), which has half-mass relaxation time  $\simeq 43\,\mathrm{Gyr}$  (Harris 1996) — 2010 edition). If NGC 2419 formed within a massive DM

 $<sup>{\</sup>color{blue} \star \ \, \text{E-mail:rodrigo.ibata@astro.unistra.fr}}$ 

halo, it is reasonable to expect that such a halo has maintained its properties almost unaltered up to the present time.

In this paper we use the recently published kinematic data set of 166 stars (Ibata et al. 2011a, hereafter Paper I) and the analysis of the stellar mass-to-light ratio  $M_*/L$ (Bellazzini et al. 2012) of the globular cluster NGC 2419 to study the DM content of this system. Paper I showed that the present kinematic and structural data on NGC 2419 can be fit acceptably well with models containing no DM; but this does not necessarily imply that models with DM cannot be as good. Previous studies have tried to put upper limits on the DM mass of NGC 2419 (Baumgardt et al. 2009; Conroy, Loeb, & Spergel 2011). Baumgardt et al. (2009) have argued that the observed velocity dispersion profile of the cluster (based on 40 stars) is not consistent with a DM halo more massive than  $M_{\rm dm}=10^7 M_{\odot}$  (assuming an isotropic stellar velocity distribution and NFW DM halo). Conroy, Loeb, & Spergel (2011) have put more stringent constraints  $(M_{\rm dm} < 10^6 M_{\odot})$ , based on the observed outermost light profile of the cluster. However, the argument of Conroy, Loeb, & Spergel (2011) relies on the hypothesis that the cluster has relaxed via two-body relaxation, which is not thought to be the case for NGC 2419.

Given the collisionless nature of NGC 2419 it is natural to explore, besides models with isotropic velocity distributions, also models with radially or tangentially biased stellar orbits. Of course it is important to exclude very radially anisotropic systems, which are radial-orbit unstable. However, in this respect it must be noted that stellar systems with massive DM halos can sustain relatively more radial kinetic energy than corresponding purely baryonic systems (Nipoti, Londrillo, & Ciotti 2002; Nipoti, Ciotti, & Londrillo 2011).

In Paper I we have shown that it is very problematic to explain the observed structure and kinematics of NGC 2419 if modified Newtonian dynamics (MOND; Milgrom 1983) is the correct theory of gravity (but see Sanders 2012 and Ibata et al. 2011b). It must be stressed that this result does not necessarily imply that NGC 2419 does not contain a substantial amount of DM. In fact, what we can infer on the basis of the Ibata et al. (2011a) results is that it is unlikely that NGC 2419 has a MOND-equivalent DM halo, i.e. a DM halo with density distribution such that the overall gravitational potential of the cluster is the same as predicted by MOND (see Milgrom 1986; Nipoti, Ciotti, & Londrillo 2011, and references therein). Of course, there is no reason to expect that the putative DM halo of this globular cluster must mimic a MOND gravitational potential, so it is quite possible that there is a significant amount of DM in NGC 2419, but that this DM is not distributed as in a MOND-equivalent halo<sup>1</sup>.

Throughout the paper we adopt the above distance to NGC 2419, which implies an angular scale of  $25.452\,\mathrm{pc}$  per arcmin. Our conclusions are virtually independent of this specific choice, because the estimated uncertainty on the distance is small ( $\sim 4\%$ ; Di Criscienzo et al. 2011). We

note that our results on the dark-to-luminous mass ratio of NGC 2419, obtained for given d and stellar mass to light ratio  $(M_*/L_V)$ , hold for all the combinations of d and  $M_*/L_V$  such that  $(M_*/L_V) \times d$  has the same value. In the present work we account for the uncertainty on  $M_*/L_V$ , which is of the order of 30% (Bellazzini et al. 2012), so it is clear that our results are not affected by the smaller uncertainties on d. Other physical properties of the cluster are listed in Table 1 of Paper I.

# 2 MODELS WITHOUT DARK MATTER

#### 2.1 Distribution function based models

Before analysing the case for the presence of dark matter in NGC 2419, it is instructive to consider models that possess only stars. In Paper I (see also Zocchi, Bertin, & Varri 2012), we presented several Michie model fits to the system in Newtonian gravity, and we showed that one of these models gives a statistically excellent representation of the cluster. However, due to high computational cost, only a small grid of 11 models were investigated in that contribution. To probe the parameter space much more finely, we re-wrote our Michie model code to allow it to be run on a parallel computer, thereby enabling us to calculate a large ensemble of Michie model fits, using a Markov-Chain Monte Carlo algorithm. This has the advantage of allowing us to properly incorporate the measurement uncertainties and also yields posterior probability distribution functions for the fitted parameters. Furthermore, we are now able to use the stellar mass to light ratio measurement of Bellazzini et al. (2012) to constrain the solutions.

The integration of the Michie models (optionally residing within within a dark matter potential) is outlined in Appendix A. We initially set the dark matter potential  $W_{\rm dm}=0$  so as to suppress that component, leaving 5 free fitting parameters: the Michie model stellar central density, the core radius, the anisotropy radius, the central potential and the stellar mass to light ratio<sup>2</sup>. For a given set of these 5 parameters, we construct a simulated surface brightness profile and the line of sight velocity distribution as a function of radius, which can be compared directly to the observations.

As in Paper I, we convolve the model velocity distributions projected onto the line of sight by the estimated Gaussian errors associated to each kinematic datum i, to give a probability distribution  $f_p(v, R_i)$  (we drop the model superscript j used in our earlier contribution, since we now consider a continuum of models defined by the above 5 parameters). The likelihood of a model then becomes:

$$\ln L = \sum_{i} \ln[f_p(v_i, R_i)] - \sum_{k} \frac{(\Sigma_p - \Sigma_k)^2}{2\delta \Sigma_k^2} + \ln\left[P\left(\frac{M_*}{L_V}\right)\right], (1)$$

where the second summation over the (k = 15) surface brightness profile data points is included to take account of the likelihood of the density profile, and the third term

<sup>&</sup>lt;sup>1</sup> It must be noted that stellar systems with MOND-equivalent halos can sustain more radial anisotropy in the central regions than MOND stellar systems (Nipoti, Ciotti, & Londrillo 2011), so, at least in principle, it is also possible that the cluster is well represented by very radially anisotropic models within a MOND-equivalent halo.

 $<sup>^2</sup>$  In Paper I, we analysed the effect on the line of sight velocity distribution of the presence of binaries in the cluster. The most likely binary fraction was found to be modest (  $\lesssim 10\%$ ), so we decided to neglect this effect in the present contribution.

is the contribution from the observed stellar mass to light  $(M_{\ast}/L_V)$  ratio.

In their analysis of recent WFC3 data of this cluster, Bellazzini et al. (2012) discuss in detail why the stellar mass to light ratio  $(M_*/L_V)$  must be constant, independent of radius. This is deduced from the uniformity of the luminosity function throughout the cluster, confirming an earlier analysis (Dalessandro et al. 2008) that reached the same conclusions based on the lack of radial segregation of the Blue Straggler Star (BSS) population<sup>3</sup>. This justifies the simplicity of the second term on the right hand side of Equation 1: the surface brightness profile should trace the projected mass density.

Having fixed the shape of the density profile, we allow for variation of its normalisation (and that of the total stellar mass  $M_*$ ) by leaving  $M_*/L_V$  as a free parameter. Bellazzini et al. (2012) found a best-fit value of  $M_*/L_V=1.5\pm0.1$ , but they argue that uncertainty in stellar evolution models allows for a range of  $1.2 \lesssim M_*/L_V \lesssim 1.7$  in the most likely value. For the probability density function P, we therefore adopt a flat distribution between  $1.2 \leq M_*/L_V \leq 1.7$ , tapered as a Gaussian of sigma 0.1 beyond these edges.

We investigated this model parameter space with a Markov-Chain Monte Carlo (MCMC) approach, using the Parallel Tempering technique (Gregory 2005). The Parallel Tempering procedure explores the parameter space at different "temperature" (i.e. smoothing) levels, which ensures that the solutions do not get stuck in local maxima. In our implementation we used 4 parallel MCMC chains, allowing swaps between the chains at random intervals of approximately 100 steps (see Gregory 2005 for a detailed description of this method). To ensure rapid convergence, the proposal step sizes of all the parameters together were refined (in lock-step) every 1000 iterations, while every 10000 steps the proposal step size of all the parameters were refined separately. We set a target acceptance ratio of 25%, so that on average one in four trial steps was accepted (this is considered to be optimal when fitting a large number of parameters, see Gregory 2005).

It is well known that systems with strong radial anisotropy are prone to the radial-orbit instability. Typically, stability criteria are expressed in terms of the Fridman-Polyachenko-Shukhman parameter  $\xi \equiv 2T_{\rm rad}/T_{\rm tan}$ , where  $T_{\rm rad}$  and  $T_{\rm tan} \equiv T_{\vartheta} + T_{\varphi}$  are the radial and tangential components of the kinetic energy tensor, respectively (Polyachenko & Shukhman 1981; Fridman & Polyachenko 1984). Here we find it convenient to use the parameter  $\xi_{\rm half}$  which

measures the same ratio, but within the half-mass radius (Nipoti, Ciotti, & Londrillo 2011). In paper I we found that, in the absence of DM,  $\xi_{\rm half}=1.5$  can be taken to separate stable and unstable models of NGC 2419. This condition is used as a prior to reject unstable solutions.

The resulting best fit from 100000 iterations of the lowest temperature chain is shown with the blue line and blue dots in Fig. 1, and is compared to the observational data. The corresponding Michie model parameter values and their uncertainties are listed in Table 1. The solution is fully compatible with the best solutions found in Paper I and Ibata et al. (2011b).

#### 2.2 Jeans equation based models

While the Michie model gives a statistically very good description of the cluster (as we have shown in Paper I), one is nevertheless left wondering how unique this solution is. In that earlier contribution we showed that isotropic Michie models (commonly referred to as King models) cannot account for the observations, but one could attempt at this stage to fit alternative models such as a Plummer, a polytrope or some other model. However, Nature need not follow these simple analytic forms. To attempt to survey the vast space of more general solutions, we have developed an algorithm that takes a different approach: we will assess instead the statistical properties of non-parametric solutions to the Jeans equation.

For a spherically-symmetric system the Jeans equation (Binney & Tremaine 2008):

$$\frac{GM(r)}{r} = -\sigma_r^2 \left[ \frac{\mathrm{d}\ln\rho}{\mathrm{d}\ln r} + \frac{\mathrm{d}\ln\sigma_r^2}{\mathrm{d}\ln r} + 2\left(1 - \frac{\sigma_\vartheta^2}{\sigma_r^2}\right) \right],\tag{2}$$

relates M(r) the cumulative mass inside a radius r to the square of the velocity dispersion profiles in the radial  $(\sigma_r^2)$  and tangential  $(\sigma_\vartheta^2)$  directions and to the logarithmic derivatives of  $\sigma_r^2$  and of the density  $(\rho)$ .

The algorithm we have developed explores these functions from the cluster centre out to the tidal radius. To sample the functions in an economical manner we found it convenient to assign one third of the radial bins to probe the inner region within two core radii with logarithmic bins. Beyond two core radii the remainder of the radial points used linear intervals. We set the value of the central velocity dispersion in the radial direction to be a model parameter. The radial velocity dispersion profile is then defined by the sequence  $\Delta \ln \sigma_r^2(r_i)$ , and the density profile is defined by the sequence  $\Delta \ln \rho(r_i)$ , where  $r_i$  are the locations of the radial bins. To interpolate these profiles into logarithmic derivatives, we assume that the functions can be approximated locally (between adjacent radial bins) by parabolas in  $\ln \sigma_r^2$ (or  $\ln \rho$ ) versus  $\ln r$ . It is worth noting that it is highly undesirable to define the profiles directly in  $\sigma_r^2$  and  $\rho$ , since this requires extremely high accuracy to avoid huge interpolation errors in the logarithmic derivatives. The remaining parameters for the dark matter free case, are the total cluster mass  $M_*$  and the stellar mass to light ratio  $M_*/L_V$ .

Our model therefore has 3 parameters unrelated to the chosen binning  $(\sigma_r^2(0), M_*, M_*/L_V)$ , plus (n-1) parameters that define the dispersion profile and n that define the density profile. We found it convenient to set the number

 $<sup>^3</sup>$  The argument that justifies a constant stellar M/L with radius is as follows: the BSS stars, which are significantly more massive than any evolving cluster star, are not observed to be radially segregated in NGC 2419, i.e. they have the same radial distribution as single stars. This should not be observed if mass segregation is at work, hence 2-body relaxation is ineffective in this cluster. Hence the stellar mix is the same at any radius, and therefore the stellar mass-to-light is the same at any radius. This argument is valid because mass segregation is expected (and observed) in most classical globular clusters, where 2-body encounters are a relevant mechanism of energy-exchange (relaxation). In less dense systems such as dwarf galaxies, the BSS population (Mapelli et al. 2009) would not allow us to draw this conclusion, as they are fully non-collisional.

# 4 Ibata et al.

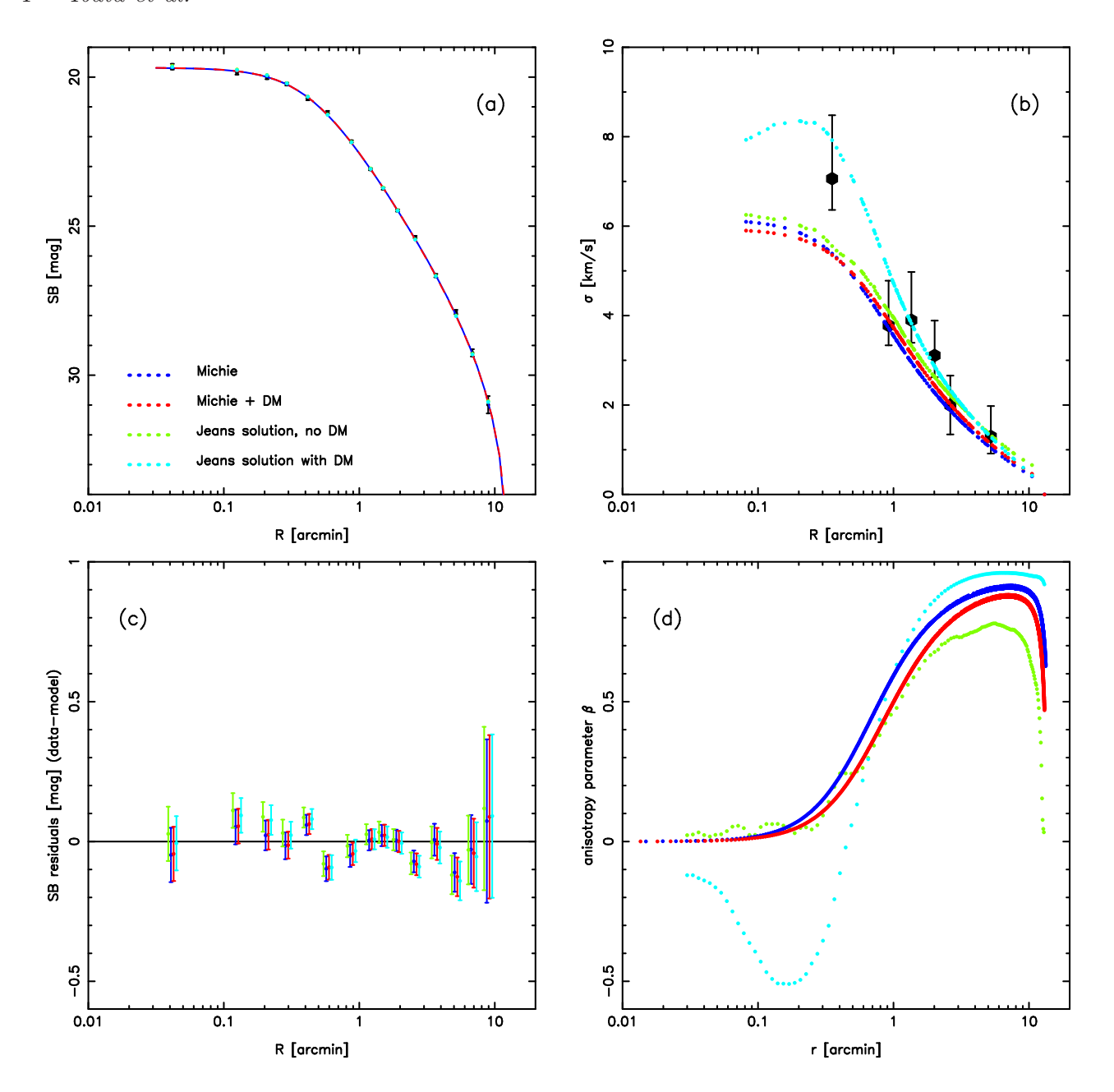


Figure 1. The surface brightness profile (a) and velocity dispersion profile (b) of the best-fit models. As described in the text, the observed data were first fit with a pure Michie model (5 free parameters) using an MCMC algorithm that explored this parameter space. The blue line in (a) shows the resulting excellent fit to the surface brightness profile. The model simultaneously also fits the kinematics, which are also shown in blue on the right-hand panel. The big hexagonal markers show a binned representation of the kinematic data, presented here *only* for visual purposes. The likelihood calculation does not use these binned values, but rather the individual kinematic measurements, the radial locations of which correspond to the radial locations of the small dots. The corresponding velocity dispersion of the model provides the ordinate value of these points. The best two-component model consisting of a Michie model to represent the stellar component and a double power law model to describe the dark matter is displayed in red. These values are almost coincident with the single (pure stellar) Michie model solution. For this composite model, a total of nine free parameters were fitted by the MCMC algorithm. The green and turquoise dots show the best non-parametric solutions derived with the MCMC Jeans equation solver. The model in green has no DM, while the turquoise model allows for a DM component. Panel (c): the surface brightness residuals between the data and the models (a small shift in radius has been applied to avoid the superposition of the points). Panel (d) shows the  $\beta$  anisotropy profile of the models. The best non-parametric model without DM (green) was derived from 1.2 × 10<sup>7</sup> MCMC trials, probing a vast parameter space of solutions; the fact its  $\beta$  profiles is very similar to that of the pure Michie model (blue) lends strong support to the use of the Michie model as a good representation of this globular cluster.

of radial bins to  $n=1+2^m$ , and certainly with n=129 the profiles are smooth and we could reconstruct a Michie model very accurately from artificial data.

The algorithm projects the 3-dimensional functions onto the line of sight, to produce a velocity dispersion profile and a surface brightness profile, from which the model likelihoods are measured using the observed data (Eqn. 1). One further assumption is made in the calculation of the likelihood: we assume that the velocity distributions are Gaussian. This assumption is not necessary for the algorithm to work, and we could have used the velocity moments of the kinematic data directly, or indeed we could have probed other parametrisations of the velocity distribution. However, it is computationally faster and avoids the errors deriving from the calculation of the moments from the data. Furthermore, the assumption is supported by the data: as we showed in Paper I, the observed distribution is consistent with a Gaussian function at all radii probed. The line of sight velocity distributions are then convolved with the uncertainty distribution appropriate for each data point.

We explore this model (260 free parameters) using a MCMC scheme<sup>4</sup>. As before, we use the Parallel Tempering technique with 4 chains to probe progressively more smoothed versions of the likelihood surface. Following Gregory (2005), this is achieved by multiplying  $\ln(L)$  by a factor  $1/m^2$ , where m is the chain number. The m=1 chain corresponds to the lowest "temperature" simulation, which is the one of primary interest.

We implemented an improvement on this method, reducing the dimensionality of the high temperature chains by redefining their radial profiles at only  $n=1+2^m$  points. Cubic interpolation (in  $\ln \sigma_r^2$  and  $\ln \rho$  versus  $\ln r$ ) between these anchor points was used to fill in intermediate values to maintain 129 radial bins in all chains. Although we attempted a simulation including a m=5 chain (i.e. with 9 radial anchor points), it was clear that the interpolation was too crude to be useful.

Some regularisation is required to tell the algorithm that it should avoid exploring very irregular profiles. This was implemented by using a mild smoothing prior on the profiles of the logarithmic derivatives.

An initial simulation with  $2\times 10^6$  iterations for each chain was run using a Metropolis-Hastings acceptance criterion. As before, all parameters were tuned in lock-step every 1000 iterations, and then refined independently every  $5\times 10^5$  iterations, so as to ensure an acceptance criterion of 25%. Finally, the 1000 best solutions from this Metropolis-Hastings algorithm were used as inputs for another  $2\times 10^6$  iteration run using an affine-invariant ensemble sampler algorithm. Our algorithm is based on the "stretch move" algorithm proposed by Goodman & Weare (2010), which we expand to use the above-described multiple "temperature" parallel chains. The simulation uses a population of 1000 "walkers" (which are non-coincident parameter space positions) which evolve from one iteration to the next, and so

sample efficiently the likelihood function. The convergence of the method was checked by running simulations from 3 very different starting positions.

While the models built from the distribution function (described in Section 2.1) are consistent by construction, this Jeans-equation based approach can yield solutions that do not have physically possible distribution functions. This is a fundamental drawback of the technique, and cannot be avoided. However, some unphysical models are eliminated by ensuring that the solutions obey the Global Density Slope-Anisotropy Inequality (GDSAI; Ciotti & Morganti 2010a,b), which is the requirement that at each radius the negative of the logarithmic slope of the stellar density distribution  $\gamma_* \equiv -\mathrm{d} \ln \rho_*/\mathrm{d} \ln r$  cannot be less than twice the local value of the anisotropy parameter,  $\gamma_*(r) \geq 2\beta(r)$ . We remind the reader that the anisotropy parameter is defined as:

$$\beta(r) \equiv 1 - \frac{\sigma_{\vartheta}^2 + \sigma_{\varphi}^2}{2\sigma_r^2},\tag{3}$$

where  $\sigma_r$ ,  $\sigma_{\vartheta}$  and  $\sigma_{\varphi}$  are, respectively, the r,  $\vartheta$  and  $\varphi$  components of the velocity-dispersion tensor. As in Section 2.1, we also impose the requirement that  $\xi_{half} < 1.5$  to ensure stability of the resulting models.

In Fig. 1 we display, in green, the surface brightness profile and velocity dispersion profile of the best solution to the Jeans equation found with this algorithm. The anisotropy profile of this solution is also shown (panel d); it is striking how closely this non-parametric solution matches the behaviour of the best-fit Michie model from Section 2.1 (shown in blue). That our Jeans equation solving algorithm should have selected this model, which is so similar to the previously-fitted Michie model, out of the vast space of possible models, lends strong support to the use of the Michie distribution function to represent the stellar component in this system. The small differences with respect to the Michie model fit in Fig. 1 can be attributed to the differences in the anisotropy profile but the driving factor is the different stellar mass to light ratio  $(M_*/L_V=1.89)$ .

# 3 MODELS WITH DARK MATTER

Following the layout of the previous section, we consider first adding dark matter to the Michie model, and then freeing M(r) in the Jeans equation so as to also allow for dark matter in those solutions.

#### 3.1 Distribution function based models

We first consider the possibility that the putative darkmatter halo can be described by the double power law density profile (Binney & Tremaine 2008):

$$\rho_{\rm dm}(r) = \frac{\rho_{\rm dm,0}}{\left(\frac{r}{r_{\rm s}}\right)^{\gamma} \left(1 + \frac{r}{r_{\rm s}}\right)^{\delta - \gamma}},\tag{4}$$

where  $\gamma$  and  $\delta$  are the two power-law indices characterising the shape of the profile,  $r_{\rm s}$  is a scale radius, and  $\rho_{\rm dm,0}$  is a reference density. In particular, when  $\gamma=1$  and  $\delta=3$  we get the Navarro, Frenk, & White (1996, NFW) model; when  $\gamma=0$  and  $\delta=3$  we get a profile with a flat inner density distribution, which is very similar to the profile proposed by Burkert (1995). For combinations of  $\gamma$  and  $\delta$  such as those

<sup>&</sup>lt;sup>4</sup> The Bayesian method we are using yields probability distribution functions for the fitting parameters, as well as information on the correlations between these parameters. In this context it is not a problem that we have more fitting parameters than data points.

mentioned above the integrated mass of the model diverges at large radii, so it is useful to introduce as an additional parameter a truncation radius  $r_{\rm vir}$  such that  $\rho_{\rm dm}=0$  for  $r>r_{\rm vir}$ . The DM mass contained within a radius r is

$$M_{\rm dm}(r) = 4\pi \int_0^r \rho_{\rm dm}(r')r'^2 dr',$$
 (5)

so the total mass of the DM halo is  $M_{\rm dm,vir}=M_{\rm dm}(r_{\rm vir})$ . If the stellar density distribution is truncated at  $r_{\rm t}$ , the kinematics of the cluster is influenced only by the mass distribution within the stellar tidal radius  $r_{\rm t}$ . It follows that our results are not sensitive to the value of  $r_{\rm vir}$ , provided that  $r_{\rm vir} \geq r_{\rm t}$ , which we assume throughout the paper (in other words, our results are not sensitive to the halo concentration  $C \equiv r_{\rm vir}/r_{\rm s}$ ). As a consequence, we define the quantity  $M_{\rm dm,t} \equiv M_{\rm dm}(r_{\rm t})$  (the DM mass contained within  $r_{\rm t}$ ), which is more useful than  $M_{\rm dm,vir}$  in order to characterise our models. In summary, our model halo is determined by specifying the following four parameters:  $\gamma$ ,  $\delta$ ,  $r_{\rm s}$  and  $M_{\rm dm,t}$ .

For the DM component, for any choice of the DM profile parameters ( $\gamma$  and  $\delta$ ) the adimensional potential can be calculated by direct integration of equation (10) as

$$W_{\rm dm}(r) = 9 \frac{\rho_{\rm dm,0}}{\rho_{*,0}} \left(\frac{r_{\rm s}}{r_{\rm c}}\right)^2 \int_{r/r_{\rm s}}^{r_{\rm t}/r_{\rm s}} \frac{1}{r'^2} \int_{0}^{r'} r''^2 \rho_{\rm dm}(r'') dr'' dr'$$

In the particular cases of a NFW ( $\gamma=1;\ \delta=3$ ) and a cored ( $\gamma=0;\ \delta=3$ ) halo the above integral admits the analytical solutions:

$$W_{\rm dm}(r) = 9 \frac{\rho_{\rm dm,0}}{\rho_{*,0}} \left(\frac{r_{\rm s}}{r_{\rm c}}\right)^2 \frac{\ln\left(1 + \frac{r}{r_{\rm s}}\right)}{\frac{r}{r_{\rm s}}}$$
(6)

when  $(\gamma = 1, \delta = 3)$ , and

$$W_{\rm dm}(r) = -\frac{9}{2} \frac{\rho_{\rm dm,0}}{\rho_{*,0}} \left(\frac{r_{\rm s}}{r_{\rm c}}\right)^2 \frac{\frac{r}{r_{\rm s}} - 2\left(1 + \frac{r}{r_{\rm s}}\right) \ln\left(1 + \frac{r}{r_{\rm s}}\right)}{\frac{r}{r_{\rm s}}\left(1 + \frac{r}{r_{\rm s}}\right)} (7)$$

when  $(\gamma = 0, \delta = 3)$ .

By incorporating this dark matter potential into the procedure described in §2.1, one can construct spherically symmetric self-consistent stellar systems, truncated at a tidal radius  $\tilde{r}_{\rm t}$ , in equilibrium in the presence of a DM halo (see also Amorisco & Evans 2011). In these models the parameters  $W_0$ ,  $r_{\rm s}/r_{\rm c}$ ,  $\tilde{r}_{\rm a}$ ,  $\rho_{\rm dm,0}/\rho_{*,0}$ ,  $\gamma$  and  $\delta$  drive the shape of the density and velocity dispersion profiles, while the values of  $\rho_{*,0}$  and  $r_{\rm c}$  determine their normalisation to physical units (see Appendix).

The stellar components of the models considered here are self-consistent by construction, but in principle it is not guaranteed that there is a positive distribution function generating the DM components. For a wide class of twocomponent models, a necessary condition for consistency is that also the DM component satisfies the GDSAI (Ciotti & Morganti 2010b). Clearly the specific form of the halo anisotropy profile is not important for the purpose of the present investigation, because the halo influences the observables only through its gravitational potential. However, we impose that in our model the halo density never increases with radius  $(d \ln \rho_{\rm dm}/d \ln r \leq 0 \text{ at all } r, \text{ i.e. } \gamma, \delta > 0)$ . This is a necessary condition for consistency only when the halo is isotropic or radially anisotropic, but we impose it as a general constraint because we think it is an astrophysically motivated assumption. However, we noted that it is not excluded that there are self-consistent tangentially biased models with d  $\ln \rho_{\rm dm}/{\rm d} \ln r < 0$  at some r.

Even if consistent, some models can be excluded because they are unstable. It has been shown that DM halo has a stabilising effect against the radial-orbit instability (Nipoti, Londrillo, & Ciotti 2002; Nipoti, Ciotti, & Londrillo 2011), so at least some models with DM halo are expected to be stable even if they have  $\xi_{\rm half} > 1.5$ . However, a full stability analysis of two-component models of NGC 2419 is beyond the purpose of the present paper, so here we conservatively assume  $\xi_{\rm half} \leq 1.5$  as a stability criterion for all the models considered in the present work. With this choice we should effectively exclude unstable models.

We proceed to examine the relative likelihoods of the two-component models built from a power-law dark matter halo and a Michie model stellar component. As in §2.1, we use a "Parallel Tempering" MCMC algorithm with 4 chains to explore the parameter space. The composite model has 9 free parameters: the stellar central density, the Michie model core radius, the anisotropy radius, the central potential, the stellar mass to light ratio, the dark matter central density, the DM characteristic radius and the DM inner and outer power-law indices. For a given set of these 9 parameters, we construct a simulated surface brightness profile and the line of sight velocity distribution as a function of radius, which can be compared directly to the observations.

Several (very weak) priors were imposed on the solutions. The stellar core radius must lie within a factor of 10 of 10.88 pc; the anisotropy radius has to lie between 0.5 and 100 core radii; the central potential parameter has to lie between 2 and 20; and the stellar mass to light ratio is required to stay within the bounds of  $0.8 < M_*/L_V < 2.1$  (i.e. within  $4\sigma$  of the flat region  $1.2 < M_*/L_V < 1.7$  stated above in Section 2.1). Furthermore, we impose that the characteristic radius of the dark matter has to lie between 25 pc and 2.5 kpc; and that the inner and outer power law exponents lie in the ranges  $0 < \gamma < 1.5$  and  $2 < \delta < 4$ . While certain black hole growth models suggest that the inner power-law slope may be higher than  $\gamma = 1.5$  (e.g., Quinlan, Hernquist & Sigurdsson 1995), this is likely to affect only the very central region of the cluster where our data do not constrain the density profile.

Figure 1 shows (in red) the most likely model found by the MCMC algorithm in  $10^6$  iterations. The solution has  $r_{\rm c}=11.4\,{\rm pc},\ r_{\rm a}=1.6r_{\rm c},\ {\rm a}$  dark matter characteristic radius of 28 pc, and  $\gamma=0.06$  and  $\delta=3.7$ . However, we were surprised to find that this model requires very little dark matter:  $M_{\rm dm}=5.0\times10^4M_{\odot}$  inside of 10′ (the approximate limit of the stellar structure), which is effectively insignificant compared to the stellar mass of  $8.1\times10^5M_{\odot}$ . Marginalising over all other parameters, we show the posterior distribution of  $M_{\rm dm}$  in Fig. 2; clearly the data appear to favour models without substantial dark matter.

To confirm this curious result, we re-ran the MCMC experiments forcing certain astrophysically-motivated parameter sets: cored DM models ( $\gamma=0$ ) and the NFW model ( $\gamma=1,\,\delta=3$ ). In an almost identical manner to the more general solution above, the model likelihoods are found to decrease strongly with increasing DM fraction. In an attempt to explore whether the MCMC algorithm was able to escape from solutions with low dark matter, we also performed an experiment forcing a massive DM component, by

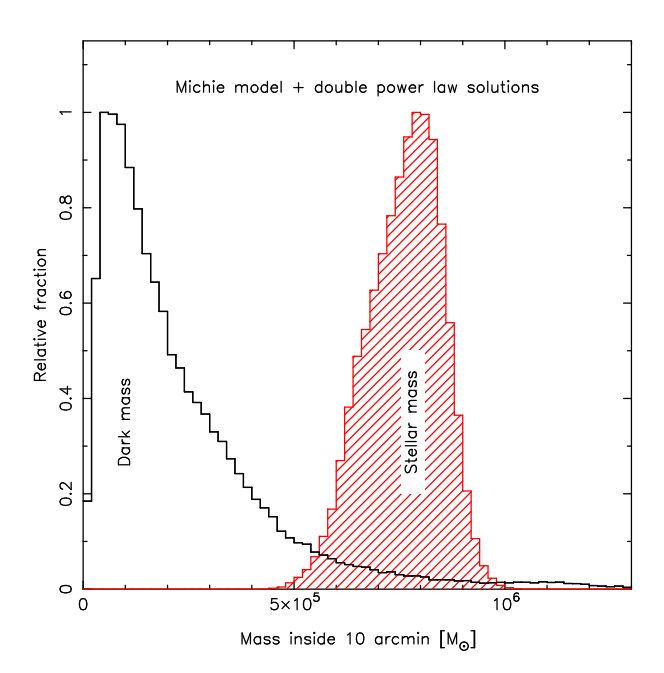


Figure 2. Unshaded histogram: the posterior distribution of the mass of the dark component inside of 10′ (the approximate size of the stellar structure) derived by the MCMC algorithm that fits a Michie model inside a dark matter halo modelled as a double power-law. The hatched histogram shows the posterior distribution of the luminous component of the cluster. Thus if we impose a Michie model on the luminous component (which as we have shown in Paper I, gives an excellent fit to the observations), the most likely solutions for the dark matter have very little mass relative to the stars. It would be natural to conclude that the cluster needs no dark component.

setting  $M_{\rm dm}>5\times10^6M_{\odot}$  as a strong prior. But again, the distribution of solutions simply clustered near this low mass limit.

We conclude from this analysis that a simple Michie model where mass traces light is actually preferred by the data over more complicated models that include the possibility of having dark matter in the form of a double power-law profile. The preference for a cored distribution turns out to be very slight - the best models with  $0.9 < \gamma < 1.1$  are only a factor of 1.4 less likely than the best model. However, solutions with some DM seem better than those without DM. This is a manifestation of the tension between stellar and dynamical mass to light ratio that was noted in Bellazzini et al. (2012) (and also in Sollima, Bellazzini & Lee 2012 in other clusters) and which is discussed further below.

# 3.2 Jeans equation based models

The paucity of dark matter implied by our MCMC survey of the likelihood surface of Michie models is compelling, since the Michie models form a fairly general family of structures, but one is again left wondering to what extent this conclusion depends on the choices of the models selected to examine both the cluster and the dark matter.

For this reason we extended our analysis to a more general set of spherical models where both the dark matter

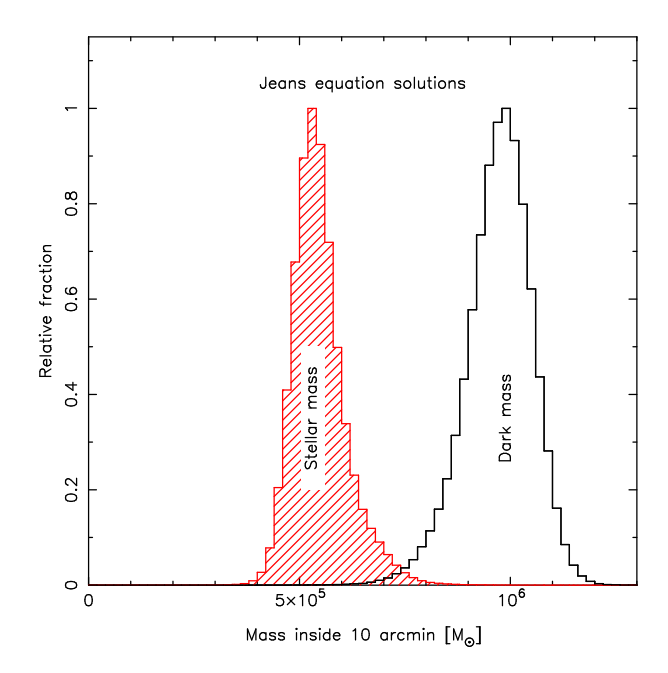


**Figure 3.** Unshaded histogram: the posterior distribution of the mass of the dark component inside of 10', but this time calculated from an MCMC algorithm that solves the Jeans equation in a non-parametric way. A total of  $1.2 \times 10^7$  MCMC iterations are presented. The difference to Figure 2 is striking: with the freedom from analytic form, the preferred solutions possess a nonnegligible dark matter component. The stellar mass of the models (hatched histogram) is approximately half that of the dark matter.

density profile and the stellar density profile are free non-parametric profiles. We reuse the non-parametric MCMC tool described in §2.2 which solves the Jeans equation, finding solutions that are consistent with the data and our priors.

However, given that we now allow for the possibility of dark matter, we require some additional information to close equation 2. To this end we have chosen to free the tangential velocity dispersion profile (in addition to  $\sigma_r^2(0)$ ,  $M_*$ ,  $M_*/L_V$ , and the profiles of  $\Delta \ln \rho$  and  $\Delta \ln \sigma_r^2$ ). We found it convenient to tabulate this profile as  $\Delta \ln \sigma_{\vartheta}^2$ , adding a further n-1 parameters to the MCMC fit, plus  $\sigma_{\vartheta}^2(0)$ . The model thus has a total of 389 free parameters.

The MCMC simulations were run in an identical manner to those described in §3.2, using again a hierarchy of 4 different "temperature" chains, each with progressively lower spatial resolution. As before, after initial runs with  $2\times 10^6$  iterations with a Metropolis-Hastings acceptance algorithm, we switched to using a population of affine-invariant ensemble samplers and reran the simulation for a further  $2\times 10^6$  iterations.

While the models built from the distribution function (described in Section 3.1) are consistent by construction (at least for as far as the stellar component is concerned), we cannot exclude that some of the two-component models considered are not generated by positive distribution functions. However, as in Section 2.2 we impose at least some necessary conditions for consistency. We additionally imposed

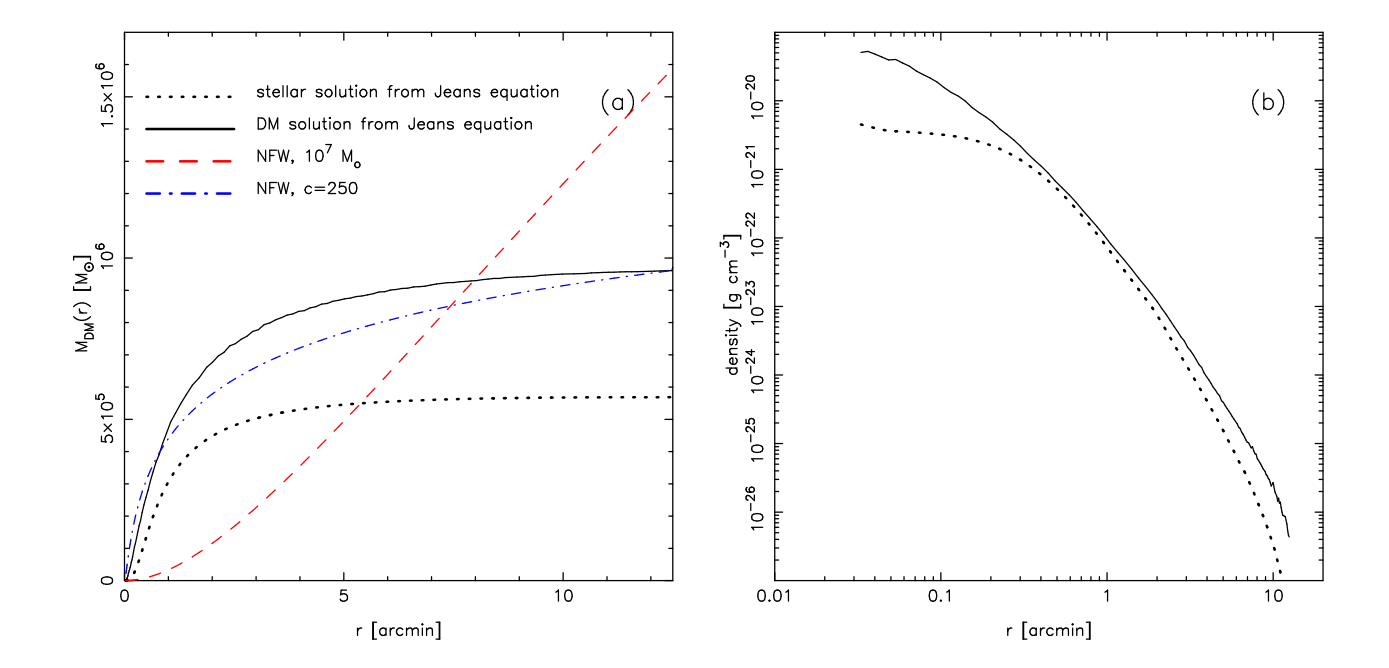


Figure 4. Panel (a): The cumulative mass profile of the dark matter component of the most likely model derived by the MCMC algorithm using the non-parametric Jeans equation method is shown with the continuous line. The dotted line shows the cumulative mass profile of the stellar component of the same solution. To first approximation the dark matter profile appears fairly similar to the stellar profile, and stands in stark contrast to cosmological expectations: the dashed line shows an NFW profile with  $M_{vir} = 10^7 M_{\odot}$ , concentration c = 23.5 and  $r_{vir} = 4.5$  kpc. The dot-dashed line shows an attempt to mimic the continuous line with an NFW profile; this however requires an extremely high concentration (c = 250), even if  $r_{vir} = 13' = 0.33$  kpc. Panel (b): the corresponding density profiles.

the prior that the dark matter density profile decreases with radius and that its logarithmic slope becomes increasingly negative with increasing radius, i.e. if the radial locations  $r_1$  and  $r_2$  are such that  $r_1 < r_2$ , the logarithmic slopes at these locations obey the condition:

$$0 > \frac{\mathrm{d} \ln \rho_{\mathrm{dm}}}{\mathrm{d} \ln r} \bigg|_{r_1} > \frac{\mathrm{d} \ln \rho_{\mathrm{dm}}}{\mathrm{d} \ln r} \bigg|_{r_2} \,.$$

This property is shared by many commonly-used models such as the Plummer sphere, the Michie (and hence King) models, the double power law models if  $\delta > \gamma$  (of which the NFW is a member), among others.

Figure 3 shows the marginalised posterior distribution of the dark matter in the solutions (unshaded histogram). The distribution peaks at  $\approx 9.7 \times 10^5 M_{\odot}$ , suggesting the presence of a significant dark matter fraction within the central 10'. The posterior distribution of the mass of the stellar component, shown with the hatched histogram, reveals that roughly half the amount in stars as dark matter appears to be present in the solutions. At first sight it would appear that we are facing a simple degeneracy between the total mass of the cluster and the mass to light ratio of the stellar population. This suspicion is reinforced by Figure 4a, which shows the cumulative mass profile in the most likely solution: the dark matter (solid line) and stars (dotted line) follow each other fairly closely (but see also the density profile in panel b). This best solution has a stellar mass to light ratio  $M_*/L_V = 1.20$ , within the acceptable range found by Bellazzini et al. (2012). This would therefore suggest that the "dark matter" component is simply the result of the al-

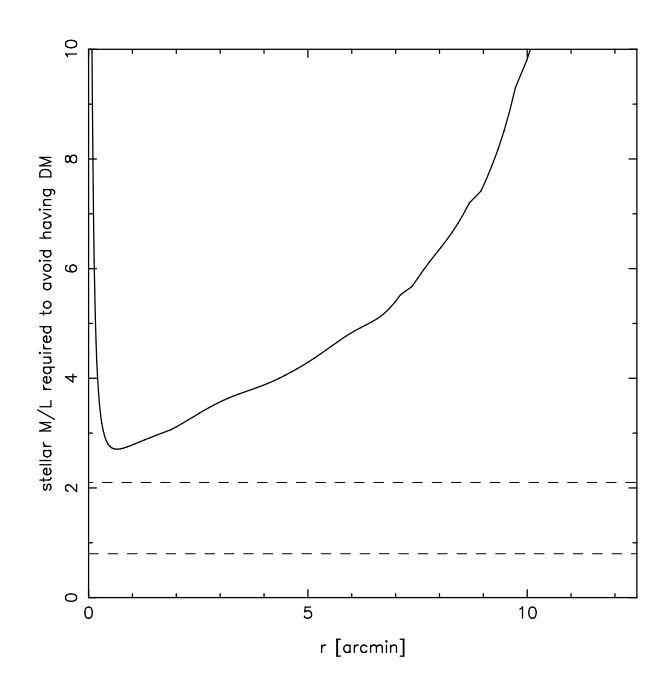


Figure 5. For the most likely non-parametric solution to the Jeans equation (shown previously in Figure 4), we calculate the stellar mass to light ratio required to eliminate the need for a dark matter component. The region between the two dashed lines marks the maximum  $(4\sigma)$  range consistent with the analysis of Bellazzini et al. (2012).

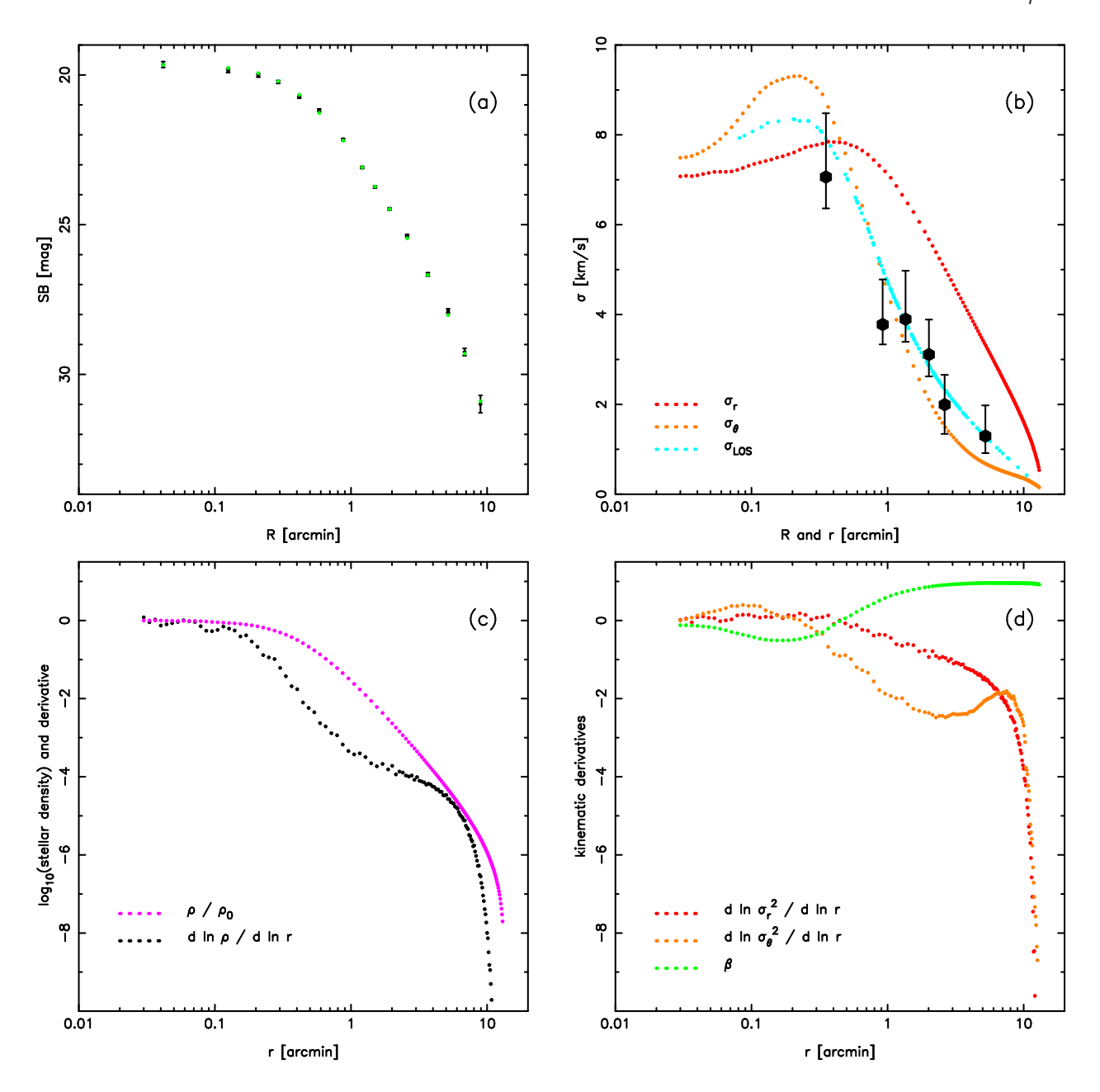


Figure 6. The most likely Jeans equation solution of NGC 2419 using the new non-parametric MCMC technique allowing for both a stellar and a dark matter component. Panels (a) and (b) show the fit to the observed surface brightness and kinematics, respectively. The data are reproduced from Figure 1. The small green dots in (a) display the excellent model fit. The non-parametric velocity dispersion profiles in the radial and tangential directions ( $\sigma_r$  and  $\sigma_\vartheta$ ) along with their line of sight projection ( $\sigma_{LOS}$ ) are displayed alongside the velocity dispersion estimates. We stress again that the *individual* star velocities were used in the likelihood calculation. The remaining profiles required for the Jeans equation solver are displayed in the bottom panels: the *stellar* density and its derivative are shown in (c), and the velocity dispersion derivatives in (d). For reference, we also show in panel (d) the anisotropy profile derived from the velocity dispersion profiles shown in (b). Note that the logarithmic derivative profiles are significantly noisier than the physical profiles. This model has a stellar mass to light ratio  $M_*/L_V = 1.20$ , which is within the acceptable range reported by Bellazzini et al. (2012).

gorithm attempting to force a constant stellar  $M_*/L_V$  over the whole radial range of the cluster.

However, this option does not appear to be possible, since it would require a  $M_*/L_V$  profile that is inconsistent with observations and other astrophysical priors, as we show in Figure 5. Here we have calculated the stellar  $M_*/L_V$  that would be required to account for the total density at a given

radius. The constraints on the uniformity of the radial profile of the  $M_*/L_V$  (Bellazzini et al. 2012), as well as the implausible  $M_*/L_V$  values beyond  $\sim 5'$  make it unlikely that the dark matter component in our Jeans equation solutions are simply due to erroneous assumptions in the  $M_*/L_V$  profile.

The best Jeans equation solution is displayed in Fig. 6; the panels also illustrate the working of the method by showing the non-parametric profiles that are refined at each Markov-Chain Monte Carlo iteration. As can be seen, the solution gives an almost perfect reproduction of the surface brightness data, and interestingly, is able to fit the full range of the kinematic data, giving a higher (and better) central velocity dispersion than any of the Michie models studied here or in Paper I. Beyond the central  $\sim 1'$ , the model is highly radially anisotropic<sup>5</sup>.

#### 4 DISCUSSION

With current data the answer to the question of whether the globular cluster NGC 2419 contains dark matter or not depends on the model (and hence one's priors) used to analyse the structure. The choice of using a Michie model for the stars plus a double power law dark matter halo, is appropriate for those who value highly dynamically self-consistent methods and who adhere strongly to cosmological expectations. The most likely solution of this composite model had  $M_{DM}(<10') = 5 \times 10^4 M_{\odot}$ , which would imply in standard  $\Lambda {\rm CDM}$  cosmology (following Navarro & Steinmetz 2000) a virial mass of  $\sim 10^5 M_{\odot}$ , roughly an order of magnitude lower than the mass of the stellar component in the cluster. The upper 99% confidence limit for the dark mass inside of 10' according to the probability distribution function in Fig. 2 is  $7.2 \times 10^5 M_{\odot}$ , and this corresponds to a virial mass of  $\sim 4 \times 10^6 M_{\odot}$ . Such a minuscule halo is some two orders of magnitude lower than expectations for the halo mass of dwarf spheroidal galaxies (Walker 2012), which have similar stellar content. Thus with this composite model the data prefers virtually no dark matter and one can rule out the possibility that the cluster is embedded at the centre of a dwarf-spheroidal-like mini-halo.

The issue of whether the cluster is located at the centre of the putative DM halo is important for the validity of the analysis presented here. However, the case should in principle be rather similar to that of the globular cluster M54 in the Sagittarius dSph, where the dynamical friction timescale for this similarly-massive globular cluster and its host halo to coincide is estimated to be  $\sim 1.5\,{\rm Gyr}$  (Bellazzini et al. 2008). The expectation therefore is that NGC 2419 should reside at the DM halo centre, if it possesses one.

The alternative analysis, using our new Jeans equation solver yields a slightly different answer. The strength of this method is that it does not require one to force a particular analytic functional form on the data. The disadvantage however, is that the resulting models are simply solutions to the Jeans equation, and so many of them are likely to be unphysical (corresponding to a non-physical distribution function) or possibly unstable, but examining the  $(\sim 10^7)$  models individually in the detail necessary to ascertain their validity would be an immense task, far beyond the scope of this contribution.

 $^5$  Recently, Zocchi, Bertin, & Varri (2012) have studied NGC 2419 (among other clusters) using so-called  $f^{(\nu)}$  models, which can represent violently relaxed systems. In their analysis (which assumes that no dark matter is present), they also manage to produce a steep central velocity dispersion profile (see their Fig. 3). Note however that their best-fit  $f^{(\nu)}$  model has  $M_*/L_V=2.4$  and is quite anisotropic ( $\xi=1.77$ ).

Nevertheless, taking the distribution in Figure 3 at face value gives a 99% upper bound to the dark matter inside of 10' of  $1.1 \times 10^6 M_{\odot}$ , which is somewhat higher than the previous method. The strong difference is that the Jeans equation solution has a 99% lower limit at  $7.5 \times 10^5 M_{\odot}$ , effectively demanding more dark matter than stars within 10'. The difference with respect to the DM-free models is that that the solutions are better able to follow the central enhancement of the velocity dispersion. In order to confirm this suspicion, we re-ran the Jeans equation simulations from §3.2 (that include dark matter), this time ignoring the most central 25 radial velocity measurements. The result was a solution very similar to that found in §2.2, with only a small dark matter fraction (mean total dark matter mass of  $1.6 \times 10^5 M_{\odot}$ inside of 10'). This experiment shows that the difference in total dark matter content between the distribution function model solution of §3.1 and the Jeans equation solution of §3.2 is due to the latter attempting to fit better the central velocity dispersion, and that it is those central stars that are driving the requirement for a (small) dark matter fraction. The MCMC algorithm accommodates this mass by changing primarily the anisotropy profile, which can be seen to be negative at r < 0.5' in Figure 6d (green dots).

It is interesting to consider which model is preferable: the best composite Michie plus double power-law model, or the best model resulting from the Jeans equation analysis? The traditional frequentist  $\chi^2$  approach is unfortunately not of much use due to the large number of parameters in the Jeans equation solver (we would simply find a negative reduced- $\chi^2$ , indicating that we have too many parameters). However, answering this question properly with Bayesian evidence is very challenging because the parameters used in the two analysis methods are very different. Indeed, it would require integrating the models over all parameter values, which would be extremely computationally costly, and is beyond the scope of the present work.

In this paper we have used kinematics measurements of NGC 2419 to test the hypothesis that this globular cluster is embedded in a massive DM halo. Another dark component that can in principle be detected via kinematics measurements is a central intermediate mass black hole (Baumgardt, Makino, & Hut 2005). However, the current kinematic sample does not allow one to set significant constraints on the mass of this putative central black hole, because it affects only the very central ( $\lesssim 0^{\prime\prime}.1)$  velocity-dispersion profile, which is barely probed by current observations.

# 4.1 Comparison with previous work

Baumgardt et al. (2009) assume that the putative halo around NGC 2419 has a NFW profile (with  $r_{\rm s}=500\,{\rm pc}$ ) and use their data to limit the dark mass inside of 500 pc to  $M_{\rm dm}(r<500\,{\rm pc})<10^7M_{\odot}$ . Given their model parameters, this corresponds to  $M_{\rm dm}(r<10')<3.9\times10^6M_{\odot}$ . In the work of Conroy, Loeb, & Spergel (2011), they also assume that the halo has a NFW profile (with  $r_{\rm s}=250\,{\rm pc}$  and  $r_{vir}=1\,{\rm kpc}$ ) and conclude that  $M_{\rm dm}(r<1\,{\rm kpc})<10^6M_{\odot}$ , which, for their model parameters, gives a very tight  $M_{\rm dm}(r<10')<2.4\times10^4M_{\odot}$ . Our results for the two component models are in reasonable agreement with these previous results. The limits provided above, are more stringent than those of Baumgardt et al. (2009), and unlike Conroy,

Loeb, & Spergel (2011), our method does not require the cluster to have suffered strong two-body relaxation, which as we have mentioned, should not have occurred in NGC 2419.

#### 5 CONCLUSIONS

We have undertaken an analysis of current data on the kinematics, structure and stellar mass to light ratio of the Galactic globular cluster NGC 2419. This distant halo cluster is a very interesting specimen to study, since it is massive and as such may have been able to maintain a residual dark matter halo over the course of its assimilation into the Milky Way. Thus NGC 2419 allows us to examine the possibility of whether (some) globular clusters formed along with (their now disrupted?) dwarf galaxy hosts within mini dark matter halos.

Our earlier analysis (Paper I) showed that a simple Michie model gives an excellent fit to the state-of-the-art measurements of the kinematics and surface brightness profile of the cluster presented in that contribution. Here we extended that study to investigate whether composite models with an additional dark matter component in the form of a generic double power-law could also be accommodated. To this end we implemented an MCMC parameter search for solutions of this composite system. The Michie distribution function is found to be highly restrictive; while it is as yet not possible to completely rule out the presence of dark matter in NGC 2419, the preferred dark matter fraction is 6% of the stellar mass within 10' (the approximate limit of the cluster), and there is virtually no room for astrophysically interesting amounts of dark matter that could hint at the formation of clusters within dark matter halos.

In a major effort to assess the model-dependence of these results we developed a new Markov-Chain Monte Carlo algorithm that solves the spherical Jeans equation using non-parametric profiles for the density and velocity dispersion profiles. A very high number of free parameters is required to follow the gradients with sufficient resolution. The code uses a hierarchy of resolutions so as to probe the parameter space as efficiently as possible. These ideas (and the software) should be applicable in the future to analyse other approximately spherical systems of interest, such as dwarf galaxies, elliptical galaxies, or galaxy clusters.

The more general Jeans equation solutions prefer a small dark matter fraction, approximately twice the stellar mass content, and at face value rule out the possibility that there is no dark matter. This last inference depends, however, on the validity of the conclusion by Bellazzini et al. (2012) that the stellar mass to light ratio is invariant with radius. For the most likely solution, the inferred dark matter profile has a very different shape to an NFW model, so it is possible that this putative dark component, if real, is related to unexpected stellar remnants (the expected remnants were taken into account by Bellazzini et al. 2012) rather than cosmological dark matter (note however, that the resolution of present-day simulations that include the relevant baryonic physics do not allow reliable predictions for the profile of dark matter mini-halos of this mass).

In their analysis, Bellazzini et al. (2012) found that assuming a 100% retention of all the dark remnants would have changed the best fit  $M_*/L_V$  from 1.49 to 1.6. Hence in

a standard scenario, changing the fraction of remnant stars will not have a sufficiently large effect to account for Fig. 5. On the other hand, as is pointed out in that contribution, all the currently available (and highly uncertain) models invoked to explain the multiple populations in GCs envisage (a) a progenitor of the present-day cluster with a baryonic mass a factor  $\gtrsim 10$  larger than today, (b) a preferential loss of first generation stars with respect to the second generation, (c) a strong difference in the radial distribution of stars of the two generations (the second one being more concentrated, as is generally observed; see Lardo et al. 2011). This complex star formation history and strong variations in the cluster potential must have occurred in the first < 500 Myr of the cluster life. It can be conceived that at this stage both (i) an anomalous production and retention of dark remnants occurred, and (ii) a radial distribution of dark remnants different from that of the light was produced and then remained un-modified in that non-collisional environment.

Therefore if the observed dark matter is of baryonic origin it is likely that it has something to do with the origin and early enrichment of the multiple populations (Cohen, Huang & Kirby 2011; Mucciarelli et al. 2012) inhabiting NGC2419. On the other hand one may imagine that we see the small remnant of a larger non-baryonic cosmological halo that was nearly completely stripped away from the cluster at early times (see, e.g. Peñarrubia, Navarro & McConnachie 2008). During the first approach to its peri-galacticon, it may have provided the potential well that allowed the cluster to retain ejecta from first generation stars.

Thus all the models we have explored turn out to have very little dark matter in their central regions, and we rule out any connection with mini dark matter halos of the mass that is associated with those in which dwarf galaxies are embedded. This conclusion, though consistent with earlier work on this particularly promising cluster, and consistent also with a large literature on more nearby systems (but which on the whole are clearly not simple isolated systems), remains puzzling. The connection between globular clusters and dwarf galaxy remnants is becoming more and more compelling (Mackey et al. 2010), so it is natural to expect that some clusters retained some of the dark matter of their former host. It is possible that this problem will only be resolved conclusively by obtaining a larger sample of distant halo clusters, but that will require observing further afield in M31, and to be feasible will require the next generation of instruments.

#### ACKNOWLEDGEMENTS

R.I. gratefully acknowledges support from the Agence Nationale de la Recherche though the grant POMMME (ANR 09-BLAN-0228). C.N. is supported by the MIUR grant PRIN2008. AS acknowledges the support of INAF through the 2010 postdoctoral fellowship grant. M.B. acknowledges the financial support of INAF through the PRIN-INAF 2009 grant assigned to the project Formation and evolution of massive star clusters, P.I.: R. Gratton.

**Table 1.** Model parameters and derived quantities for the four families of models investigated in this contribution. Where possible, we report the mean value and root mean square dispersion of the MCMC solutions. Due to the construction of our Jeans equation algorithm, the stellar central density is expensive to calculate at every MCMC iteration, so we report only the values of the most likely solution. Furthermore, the posterior probability distribution for the dark mass in Fig. 2 is highly skewed, so we only report the most likely value for that model.

	Michie	Jeans without DM	Michie + DM	Jeans with DM
stellar central density $(M_{\odot} \text{ pc}^{-3})$	$57.3 \pm 4.8$	74.4 (best value)	$59.2 \pm 10$	66.9 (best value)
stellar core radius (pc)	$12.6 \pm 0.6$		$10.8 \pm 0.5$	***
anisotropy radius (pc)	$14.2 \pm 2.3$		$18.3 \pm 2.7$	•••
central potential	$3.6 \pm 0.4$		$4.7 \pm 1.1$	•••
stellar $M/L$	$1.72 \pm 0.11$	$1.89 \pm 0.07$	$1.62 \pm 0.17$	$1.15 \pm 0.12$
Stellar mass $(10^5 M_{\odot})$	$8.1 \pm 0.2$	$9.0 \pm 0.1$	$7.6 \pm 0.8$	$5.5 \pm 0.6$
Dark mass $(10^5 M_{\odot})$	0	0	0.5 (best value)	$9.7 \pm 0.8$

#### APENDIX A

The distribution function proposed by Michie (1963) has the following phase-space form:

$$f(E, L) = f_0 \exp\left(-\frac{L}{2\sigma_{\rm K}^2 r_{\rm a}^2}\right) \left[\exp\left(-\frac{E}{\sigma_{\rm K}^2}\right) - 1\right],$$

$$f(r, v_{\rm r}, v_{\rm t}) = f_0 \exp\left[-\frac{v_{\rm t}^2}{2\sigma_{\rm K}^2} \left(\frac{r}{r_{\rm a}}\right)^2\right] \times \left[\exp\left(-\frac{v_{\rm r}^2 + v_{\rm t}^2}{2\sigma_{\rm K}^2} - \frac{\psi}{\sigma_{\rm K}^2}\right) - 1\right],$$
(8)

where E and L are the energy and angular momentum per unit mass, respectively,  $\psi$  is the effective potential defined as the difference between the cluster potential (including the contribution of both stars and the dark matter — the latter component will be added in Section 3.1) at a given radius r and the potential at the cluster tidal radius ( $\psi = \phi - \phi_{\rm t}$ ),  $f_0$  is a normalization coefficient factor,  $\sigma_{\rm K}$  is a reference velocity dispersion,  $v_{\rm t}$  and  $v_{\rm r}$  are the radial and tangential component of the velocity and  $r_{\rm a}$  is the anisotropy radius: the velocity distribution tends to be isotropic at  $r < r_{\rm a}$  and radially anisotropic at  $r > r_{\rm a}$ .

The density and the radial and tangential components of the velocity dispersion can be derived by integrating the above distribution function:

$$\rho_*(r) = 4\pi \int_0^{\sqrt{-2\psi}} \int_0^{\sqrt{-2\psi - v_r^2}} v_t f(r, v_r, v_t) dv_t dv_r,$$

$$\sigma_r^2(r) = \frac{4\pi}{\rho_*(r)} \int_0^{\sqrt{-2\psi}} v_r^2 \int_0^{\sqrt{-2\psi - v_r^2}} v_t f(r, v_r, v_t) dv_t dv_r,$$

$$\sigma_t^2(r) = \frac{4\pi}{\rho_*(r)} \int_0^{\sqrt{-2\psi}} \int_0^{\sqrt{-2\psi - v_r^2}} v_t^3 f(r, v_r, v_t) dv_t dv_r.$$

It is convenient to work with the dimensionless quantities

$$\begin{split} \zeta &= \frac{v_{\rm r}^2}{2\sigma_{\rm K}^2}, \, \eta = \frac{v_{\rm t}^2}{2\sigma_{\rm K}^2}, \\ \tilde{\rho}_* &= \frac{\rho_*}{\rho_{*,0}}, \ \tilde{r} = \frac{r_{\rm c}}{r_{\rm c}}, \\ W &= -\frac{\psi}{\sigma_{\rm K}^2}, \ \tilde{r}_{\rm a} = \frac{r_{\rm a}}{r_{\rm c}}, \end{split}$$

where  $\rho_{*,0}$  is the central cluster density and

$$r_{\rm c} \equiv \left(\frac{9\sigma_{\rm K}^2}{4\pi G \rho_{*,0}}\right)^{1/2}$$

is the core radius (King 1966). The above equations can be then written as

$$\begin{split} \tilde{\rho}_{*}(\tilde{r}) &= \frac{\int_{0}^{W} \zeta^{-\frac{1}{2}} \int_{0}^{W-\zeta} e^{-\frac{\eta \tilde{r}^{2}}{\tilde{r}_{a}^{2}}} (e^{W-\eta-\zeta}-1) \; \mathrm{d}\eta \; \mathrm{d}\zeta}{\int_{0}^{W_{0}} \zeta^{-\frac{1}{2}} \int_{0}^{W_{0}-\zeta} e^{-\frac{\eta \tilde{r}^{2}}{\tilde{r}_{a}^{2}}} (e^{W_{0}-\eta-\zeta}-1) \; \mathrm{d}\eta \; \mathrm{d}\zeta}, \\ \sigma_{\mathrm{r}}^{2}(\tilde{r}) &= \frac{2\sigma_{\mathrm{K}}^{2} \int_{0}^{W} \zeta^{\frac{1}{2}} \int_{0}^{W-\zeta} e^{-\frac{\eta \tilde{r}^{2}}{\tilde{r}_{a}^{2}}} (e^{W-\eta-\zeta}-1) \; \mathrm{d}\eta \; \mathrm{d}\zeta}{\int_{0}^{W} \zeta^{-\frac{1}{2}} \int_{0}^{W-\zeta} e^{-\frac{\eta \tilde{r}^{2}}{\tilde{r}_{a}^{2}}} (e^{W-\eta-\zeta}-1) \; \mathrm{d}\eta \; \mathrm{d}\zeta}, \\ \sigma_{\mathrm{t}}^{2}(\tilde{r}) &= \frac{2\sigma_{\mathrm{K}}^{2} \int_{0}^{W} \zeta^{-\frac{1}{2}} \int_{0}^{W-\zeta} e^{-\frac{\eta \tilde{r}^{2}}{\tilde{r}_{a}^{2}}} (e^{W-\eta-\zeta}-1) \; \mathrm{d}\eta \; \mathrm{d}\zeta}{\int_{0}^{W} \zeta^{-\frac{1}{2}} \int_{0}^{W-\zeta} e^{-\frac{\eta \tilde{r}^{2}}{\tilde{r}_{a}^{2}}} (e^{W-\eta-\zeta}-1) \; \mathrm{d}\eta \; \mathrm{d}\zeta}, \end{split}$$

which can be solved once the potential  $W(\tilde{r})$  is known. This last quantity can be written as the sum of the stellar and DM contributions  $W=W_*+W_{\rm dm}$ . Both contributions must obey independently the Poisson equation

$$\nabla^2 \phi_i = 4\pi G \rho_i,$$

$$\frac{\mathrm{d}^2 W_i}{\mathrm{d}\tilde{r}^2} + \frac{2}{\tilde{r}} \frac{\mathrm{d}W_i}{\mathrm{d}\tilde{r}} = -9\tilde{\rho}_i.$$
(10)

Here, the subscript i refers to either stars or DM. For the stellar component we leave  $W_0$  as a free parameter and solve equation (10) adopting the boundary conditions at the center

$$W_{*,0} = W_0 - W_{\text{dm},0},$$
  
 $\frac{dW_{*,0}}{d\tilde{r}} = 0.$ 

Equations (9) and (10) can be integrated numerically to derive the three-dimensional density profile, and the radial and tangential velocity dispersion profiles. Finally, the above profiles have been projected on the plane of the sky to obtain the surface mass density

$$\Sigma_*(R) = 2 \int_R^{\tilde{r}_t} \frac{\tilde{\rho}_* \tilde{r} d\tilde{r}}{\sqrt{\tilde{r}^2 - R^2}}$$
(11)

and the line-of-sight velocity dispersion

$$\sigma_{\rm V}^2(R) = \frac{1}{\Sigma_*(R)} \int_R^{\tilde{r}_{\rm t}} \frac{\tilde{\rho}_* \left[ 2\sigma_{\rm r}^2 \left( \tilde{r}^2 - R^2 \right) + \sigma_{\rm t}^2 R^2 \right] d\tilde{r}}{\tilde{r} \sqrt{\tilde{r}^2 - R^2}} \,. \tag{12}$$

As described in Section 2.1, the full likelihood analysis performed here requires for each model the knowledge of the distribution of projected velocities (not only its second-order moment). This function can be calculated as

$$f_p(v,R) = \int_0^{r_t} \frac{\rho_*(r)r}{\sqrt{r^2 - R^2}} \int_0^{\sqrt{-2\psi - v^2}} \times \int_0^{\sqrt{-2\psi - v^2 - v_x^2}} f(r, v_r', v_t') \, dv_y dv_x dr,$$
(13)

adopting the following change of variables

$$v'_{\rm r} = v \sin \alpha + v_x \cos \alpha,$$
  
 $v'_{\rm t} = [(v \cos \alpha - v_x \sin \alpha)^2 + v_y^2]^{1/2},$ 

where  $\alpha = \arccos(R/r)$ .

# REFERENCES

Amorisco N. C., Evans N. W., 2011, MNRAS, 411, 2118 Baumgardt H., Makino J., Hut P., 2005, ApJ, 620, 238 Baumgardt H., Mieske S., 2008, MNRAS, 391, 942 Baumgardt H., Côté P., Hilker M., Rejkuba M., Mieske S., Djorgovski S. G., Stetson P., 2009, MNRAS, 396, 2051 Bekki, K., Yong, D., 2012, MNRAS, 419, 2063 Bellazzini, M., Dalessandro, E., Sollima, A., Ibata, R., 2012, MNRAS, 423, 844

Bellazzini M., Ibata, R., Chapman, S., Mackey, D., Monaco, L., Irwin, M., Martin, N., Lewis, G., Dalessandro, E., 2008, AJ, 136, 1147

Binney J., Mamon G.A., 1982, MNRAS, 200, 361

Binney J., Tremaine S., 2008, Galactic Dynamics 2nd Ed., Princeton University Press, Princeton

Bradford J. D., et al., 2011, ApJ, 743, 167

Burkert A., 1995, ApJ, 447, L25

Ciotti L., Morganti L., 2010a, MNRAS, 401, 1091

Ciotti L., Morganti L., 2010b, MNRAS, 408, 1070

Cohen, J., Huang, W., Kirby, E., 2011, ApJ, 740, 60

Conroy C., Loeb A., Spergel D., 2011, ApJ, 741, 72

Dalessandro, E., Lanzoni, B., Ferraro, F., Vespe, F., Bellazzini, M. Rood, R., 2008, ApJ, 681, 311

Di Criscienzo M., et al., 2011, AJ, 141, 81

Fridman A. M., Polyachenko V. L., 1984, Physics of Gravitating Systems. Springer, New York

Goodman, J., Weare, J., 2010, Comm. App. Math. Comp. Sci., 5, 65

Gregory, P., 2005, Bayesian Logical Data Analysis for the Physical Sciences. Cambridge University Press

Harris W. E., 1996, AJ, 112, 1487

Heggie D. C., Hut P., 1996, IAUS, 174, 303

Ibata R., Sollima A., Nipoti C., Bellazzini M., Chapman S. C., Dalessandro E., 2011a, ApJ, 738, 186

Ibata R., Sollima A., Nipoti C., Bellazzini M., Chapman S., Dalessandro E., 2011b, ApJ, 743, 43

Lardo, C., Bellazzini M., Pancino, E., Carretta, E., Bragaglia, A., Dalessandro E., 2011, A&A, 525, 114

Mackey, D., Huxor, A., Ferguson, A., Irwin, M., Tanvir, N., McConnachie, A., Ibata, R., Chapman, S., Lewis, G., 2010, ApJ, 717, 11

Mapelli M., Ripamonti E., Battaglia G., Tolstoy E., Irwin M. J., Moore B., Sigurdsson S., MNRAS, 396, 1771

Mashchenko S., Sills A., 2005a, ApJ, 619, 243

Mashchenko S., Sills A., 2005b, ApJ, 619, 258

Merritt D., 1985, AJ, 90, 1027

Michie R. W., 1963, MNRAS, 125, 127

Milgrom M., 1983, ApJ, 270, 365

Milgrom M., 1986, ApJ, 306, 9

Moore B., 1996, ApJ, 461, L13

Mucciarelli, A., Bellazzini, M., Ibata, R., Merle, T., Chapman, S., Dalessandro, E., Sollima, A., 2012, arXiv:1208.0195

Navarro J. F., Steinmetz, M., 2000, ApJ, 538, 477

Navarro J. F., Frenk C. S., White S. D. M., 1996, ApJ, 462, 563 (NFW)

Nipoti C., Londrillo P., Ciotti L., 2002, MNRAS, 332, 901 Nipoti C., Ciotti L., Londrillo P., 2011, MNRAS, 414, 3298

Osipkov L. P., 1979, Soviet Astron. Lett., 5, 42

Peebles P. J. E., 1984, ApJ, 277, 470

Peñarrubia, J., Navarro, J., McConnachie, A., 2008, ApJ, 673, 226

Polyachenko V. L., Shukhman I. G., 1981, SvA, 25, 533 Quinlan G. D., Hernquist L., Sigurdsson S., 1995, ApJ, 440, 554

Saitoh T. R., Koda J., Okamoto T., Wada K., Habe A., 2006, ApJ, 640, 22

Sanders, R., 2012, MNRAS, 419, 6

Sollima, A., Bellazzini, M., Lee, J.-W., 2012, arXiv:1206.4828

Walker, 2012, arXiv:1205.0311

Zocchi A., Bertin G., Varri A. L., 2012, A&A, 539, A65